Electric response of topological dipoles in nematic colloids with twist-bend nematic droplets as the dispersed phase

K. S. Krishnamurthy ⬡,[*] D. S. Shankar Rao, Madhu B. Kanakala ⬡, and Channabasaveshwar V. Yelamaggad
Centre for Nano and Soft Matter Sciences, Survey No. 7, Shivanapura, Bangalore 562162, India

Colloidal systems comprising solid or fluid particles dispersed in nematic monodomains are known to be a convenient means to study topological defects. Recent experiments have shown that twist-bend nematic (N_{TB}) droplets in a nematic matrix act as colloidal particles that lead to the formation of elastic dipoles, quadrupoles, and their ordered clusters. In this study, we examine the effect of low-frequency ($f \sim$ mHz) electric fields on such defect configurations. We find that (i) the hyperbolic hedgehogs of elastic dipoles shift toward the negative electrode in static fields and perform oscillatory motion in AC fields, indicating the presence of nonvanishing flexoelectric polarization in the field-free state; (ii) the elastic dipoles, propelled by forces of backflow due to coupled flexoelectric and dielectric distortions, drift uniformly along their axes with the N_{TB} drops in lead; (iii) the translational velocity v_d increases linearly with both f and the diameter of N_{TB} drops; and (iv) with increasing applied voltage U, $v_d(U)$ exhibits a monotonic, slightly nonlinear variation at $f \leqslant 200$ mHz, tending toward linearity at higher frequencies.

I. INTRODUCTION

A planarly aligned nematic monodomain, with μm-size spherical solid or fluid particles dispersed in it, is perhaps the simplest of colloidal systems with which to realize a rich variety of topological defect structures and to study their elastic interactions [1–4]. When the preferred axis of orientation in the far-field nematic, specified by an apolar unit vector (director) $\mathbf{n}_o \equiv -\mathbf{n}_o$, differs from the axis preferred at the particle surface, singularities may be enforced in the director distribution. For particles of radius R, this happens when homeotropic anchoring is favored at the surface and $R \gg k/W$, k and W denoting, respectively, the appropriate elastic and anchoring coefficients. With strong anchoring ($W = 10^{-4}$ J m^{-2}) and a typical k value (10 pN), a microsphere would then act as a radial hedgehog of topological charge $+1$, generating in its vicinity a hyperbolic antidefect of charge -1. The elastic dipole so formed is characterized by an axially symmetric director field $\mathbf{n(r)}$ [1]. Instead of the -1 point defect, depending on the particle size, surface anchoring strength, and other factors, a loop disclination (Saturn ring) of strength $-1/2$ may form in the equatorial plane of the particle, rendering the associated $\mathbf{n(r)}$ to be of quadrupolar symmetry [5,6]. Such dipoles and quadrupoles are the key elements of which many complex topological structures—such as ordered chains of dipoles and quadrupoles [7,8], entangled Saturn ring geometries of significance in knot theory [9–11], and colloidal crystals of relevance in photonics [8,12]—are built. The self- or directed assembling of colloidal particles and their companion defects is governed by strong, anisotropic, long-range elastic forces

that resemble electrical forces [13,14] and come into play whenever the distorted director fields overlap.

The motion of colloidal particles, apart from its occurrence due to director gradients, may also be driven by an external field. In particular, in an applied electric field **E**, there exist several mechanisms—such as dielectrophoresis [15], linear and nonlinear electrophoreses [16], the Quincke rotational effect [17], ordoelectric polarization (arising from order parameter gradients) [18], and backflows consequent on time evolution and decay of dielectric [19,20] and flexoelectric [21] instabilities—by which the particle transport may occur. Refs. [22,23] provide comprehensive reviews of important advances in electrokinetics in what are described therein as active liquid crystal colloids. The present study is specifically concerned with an electrokinetic phenomenon seen in topological dipoles because of backflows associated with flexodielectric hybrid deformation of $\mathbf{n(r)}$. Backflow-induced transport of spherical silica particles dispersed in nematic E7 has been previously observed and analyzed by numerical simulation [19]; the backflow here is, in turn, caused by periodic growth and decay of Freedericksz (dielectric) deformation in the whole of nematic matrix excited by a pulsed high-frequency field. While there exists also a numerical simulation study dealing with backflows in flexoelectric nematic layers involving converse flexoelectric distortion [21], effect of such backflows on elastic dipoles does not appear to have been studied either in theory or experiment. Apart from this, even in the field-free state, the splay-bend curvature strains inherent in the structure of a topological dipole may produce a non-vanishing flexoelectric polarization that becomes manifest in an external field. Our low-frequency electric field experiments concerning polarity-sensitive dynamical effects in topological dipoles reveal both translocation of hyperbolic defects within the dipoles and rectilinear transport of dipoles along their axes
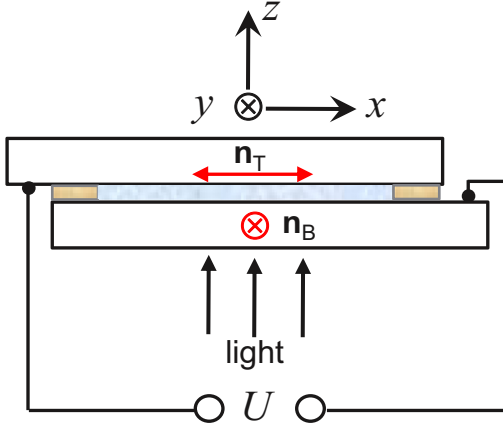
---

[*]murthyksk@cens.res.in

FIG. 1. Sample geometry showing a 90° twist cell with nematic directors $\mathbf{n}_T$ and $\mathbf{n}_B$ at top and bottom substrates; in untwisted planar cells, alignment is uniformly along x. Applied voltage U is taken positive when the field acts along z.

FIG. 2. (a) A typical topological dipole existing in the N-N_{TB} biphasic region of C-TA5 in a planar cell, viewed between crossed polarizers P and A. The N_{TB} droplet, with its twist axes emanating radially from a point singularity of strength $+1$, generates a satellite -1 defect, with hyperbolic field lines around it in the nematic with its far-field director $\mathbf{n}$ along x (in the surrounding dark region). (b) Schematic of the director field around the N_{TB} droplet. The elastic dipole $\mathbf{p}_t$ is along $-x$; as the present study reveals, the associated flexoelectric dipole $\mathbf{p}_e$ acts oppositely, along $+x$.

due to deformations *localized* at hyperbolic defect sites, while the far-field nematic matrix remains in the base state. These results are from our electrooptic observations on a recently reported [24] uncommon variety of dipoles, each made of a twist-bend nematic (N_{TB}) drop and a satellite hyperbolic hedgehog formed in the surrounding nematic fluid. Our presentation of the results in Sec. III is supplemented by eight video clips, some optical textures and related notes; these are accessible in Supplemental Material, SM [25].

II. EXPERIMENTS

Binary systems studied were of 1″,7″-bis(4-cyanobiphenyl-4′-yl)heptane (CB7CB) mixed with a small quantity of one of the surfactant materials: 1-tetradecanoic acid (TA), 2-octadecoxypropanol (OP), 2-docosanoxypropanol (DP), and 2-hexadecoxybutanol (HB); these mixtures are referred to as C-TAi, C-OPi, C-DPi, and C-HBi, where C stands for CB7CB, and i for the concentration, in wt %, of the amphiphile. The i value was usually kept low, being either 3 or 5 wt %, to avoid phase separation occurring at higher concentrations. It is important to note here that all the binary systems studied were of similar phase behavior, involving the two nematic mesophases N and N_{TB}, with their biphasic region extending over a few °C, around 92 °C. Our experiments with several surfactants were aimed at examining the relative stabilities of different topological defect configurations. In so far as the electrical responses discussed in this study are concerned, all the mixtures were quite alike. For convenience of discussion, the sample geometry is depicted in Fig. 1. We specify the orientation of polarizers as $P(\alpha)$-$A(\beta)$, where α and β (in degrees) are, respectively, the angles made by the transmission axes of the polarizer P and analyzer A relative to x. Optical textures were examined using a Carl-Zeiss Axio Imager.M1m polarizing microscope with an AxioCam MRc5 digital camera. Textures in monochromatic light were obtained using the confocal laser scanning accessory (LSM5) of the microscope in the transmission mode. The sample cells
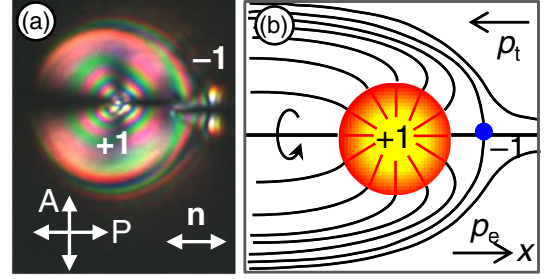
(from M/s AWAT, Poland) were sandwich type with a gap $L \approx 20\,\mu m$, and made of indium tin oxide electrodes, coated with polyimide, and buffed unidirectionally to ensure a strong planar anchoring of the nematic director $\mathbf{n}$ at the substrates; sample temperature T was maintained accurate to $\pm 0.1\,°C$ using an Instec HCS402 hot stage connected to an STC200 temperature controller. For electric field studies, a Stanford Research Systems function generator (DS345) coupled to an FLC Electronics voltage amplifier (model A800) was used. Field frequency f and rms voltage U were measured with a Keithley-2002 multimeter. The size of N_{TB} drops is indicated by D_y, the principal axis of the drop along y.

III. RESULTS AND DISCUSSION

A. Flexoelectrically induced dipole reorientation

Our recent studies [24] on binary mixtures of the twist-bend nematic CB7CB and the amphiphile TA have shown that, in the N-N_{TB} coexistence region, the N_{TB} phase nucleates sporadically in the homogeneous nematic matrix as droplets that grow into large flattened spherulites, with their diameter in the layer plane often extending to hundreds of μm. The drops act as radial hedgehogs, with the N_{TB} helix axis radially disposed around a point singularity of charge $+1$. The overall topological charge neutrality is achieved, as in usual nematic colloids, through generation of a hyperbolic nematic hedgehog of strength -1, in the vicinity of each N_{TB} drop (Fig. 2). The director field associated with the resulting dipoles is cylindrically symmetric about the dipole axis x. The distortion linked to this field produces the flexoelectric (flexo, for short) polarization $\mathbf{P}_f$ given by

$$\mathbf{P}_f = e_s \mathbf{n}(\nabla \cdot \mathbf{n}) + e_b \mathbf{n} \times (\nabla \times \mathbf{n}),$$

where e_s and e_b are the splay and bend flexoelectric coefficients, respectively [26]. While the components of $\mathbf{P}_f$ in the plane orthogonal to the dipole axis cancel out due to the cylindrical symmetry, the axial components, as this study reveals, do not fully compensate because of left-right asymmetry. A
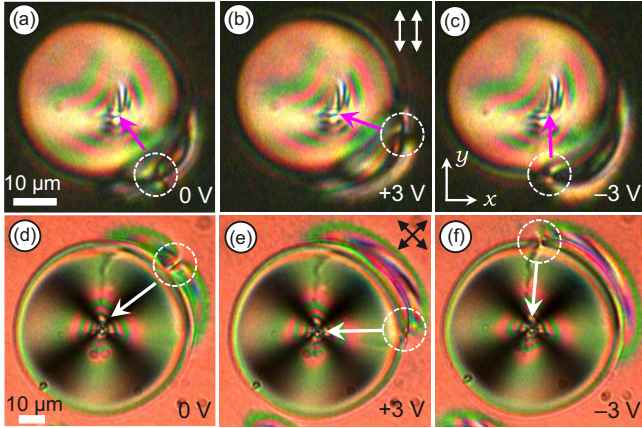
FIG. 3. Drift of the hyperbolic defect in a 90° twisted layer of C-HB3 subjected to a static field. In the field-free state, the dipoles are diagonally oriented along the midplane director with respect to the x axis. Regardless of the initial dipole orientation, positive voltages produce, as a rule, the movement of the -1 defect around the drop toward the x axis by the shortest path; and under negative voltages, by contrast, the defect glides toward the y axis. The angular displacement increases nonlinearly with U. $D_y = 40 \,\mu$m (a) and 76 μm (b).

FIG. 4. Dependence on applied voltage U of the angle ϕ by which the -1 defect drifts. Open and filled squares correspond, respectively, to the drift toward the x and y axes. The continuous lines are quadratic polynomial fits. Above 3.5 V, the surrounding nematic undergoes the Bobylev-Pikin volume instability, characterized by the formation of periodic diagonal domains.

net flexoelectric dipole moment $\mathbf{p}_e$ thus comes to exist along x and opposite the topological dipole $\mathbf{p}_t$.

A strong indication of nonvanishing flexoelectric polarization accompanying the elastic dipole comes from the instabilities induced by static and low-frequency electric fields at hyperbolic defect sites formed in a 90° twisted nematic layer. In the field-free or base state, an elastic dipole $\mathbf{p}_t$ lying in the midplane xy of a twist cell may assume one one of the two degenerate orientations defined by the midplane director $\mathbf{n}_M$. Thus there exist four possible dispositions of $\mathbf{p}_t$ from the two oppositely twisted regions. For example, the dipole in Fig. 3(a), from a right-handed region, is at approximately 135° relative to x; and that in Fig. 3(d), from a left-handed region, is at 225°. On applying a small static voltage in the range 2–4 V, while the N_{TB} and far-field nematic regions remain undisturbed (with the birefringence colors therein unvarying), the hyperbolic hedgehog undergoes a *polarity-dependent* destabilization. For example, in Fig. 3(b) showing the dipole subjected to a positive U, the -1 defect appears, in top view, to go around the N_{TB} drop anticlockwise toward the x axis. This is true regardless of how $\mathbf{p}_t$ is initially oriented, as may be seen, for example, in Fig. 3(e), where the motion is clockwise. In other words, the sense of rotation of the negative defect corresponds to the shortest path in approaching the x axis under a positive field. Subjected to a negative field, the defect drifts toward the y axis, again by the shortest route, as in Figs. 3(c) and 3(f). As U is gradually increased, the angle ϕ through which the defect drifts in the layer plane also increases, with $\phi(U)$ being a quadratic polynomial. In measurements made on the same dipole, the ϕ values for positive and negative fields, at any given $|U|$, were found to be very different, although the trend of variation $\phi(U)$ remained the same (Fig. 4). This is probably due to interactions between neighboring dipoles causing observable deviations from the
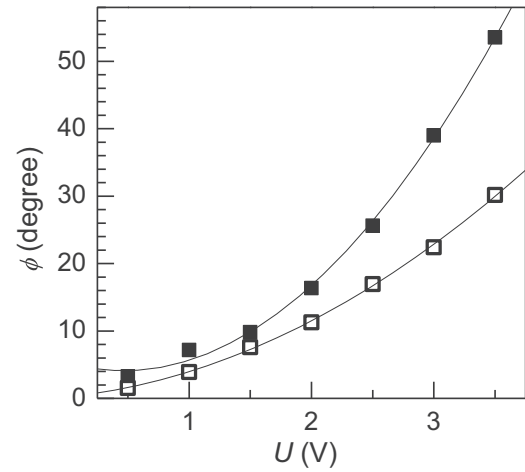
expected initial diagonal alignment (along $\mathbf{n}_M$) of the dipole under observation.

The field-induced motion of the hyperbolic defect may be qualitatively understood as due to the electric torque $\mathbf{p}_e \times \mathbf{E}$ on the flexodipole causing it to reorient toward the field direction and contribute negatively to free energy, by $-\mathbf{p}_e \cdot \mathbf{E}$. This reorientation takes place in a manner that the horizontal component of $\mathbf{p}_e$ remains in the direction of local nematic director (Fig. 5). Additionally, it is possible that the drift involves electrohydrodynamic interactions since flexodipoles may attract ionic impurities that respond to Coulombic forces.

The motion of the defect in a low-frequency (mHz) field is, expectedly, oscillatory. This is exemplified in video V1 available in Supplemental Material, SM [25] showing the defect motion under a sine wave field with $f = 20$ mHz and rms voltage $U = 2.5$ V; at the start of the movie clip, the voltage is negative, the drift taking place toward the y axis. Maximum amplitude of clockwise (anticlockwise) drift occurs at the peak positive (negative) voltage ($|U_p| = 3.5$ V). In a low-frequency square wave (SQW) field, the maximum drift occurs soon after each polarity change. In addition, when U is sufficiently large, at each polarity reversal, a periodic instability appears transiently in the surrounding nematic medium that remains homogeneous during field constancy. This phenomenon is illustrated in Fig. 6.

Polarity-sensitive, patterned instabilities arising momentarily at field reversals, such as in Fig. 6 (see video V2 in SM [25]), are a general phenomenon encompassing dielectric [27], flexoelectric [28], and electroconvective modulations [29,30]. For a qualitative appreciation of the effect, we may consider the electric field distribution in a planar nematic with an electrical conductivity on the order of μS/m, as in the case of the samples under study. Under an applied field $E = U/d$, assuming the polyimide coatings on the substrates to block any charge injection, the nematic, acting as a weak electrolyte with a high concentration of ionic impurities, develops dif-
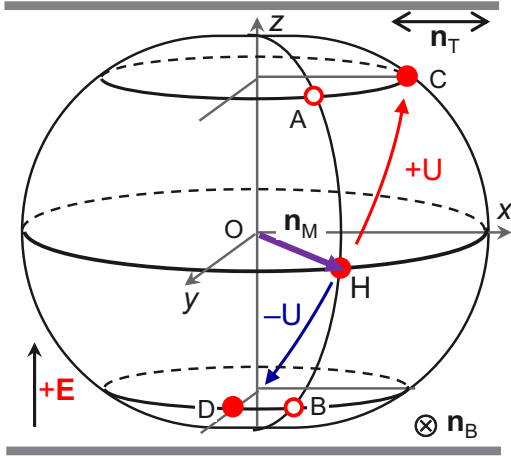
FIG. 5. Schematic to visualize the drift of a hyperbolic hedgehog under an applied static field. A flattened spherulitic N_{TB} drop between two substrates (thick gray lines) with a $+1$ topological charge, coupled to a hyperbolic hedgehog of opposite charge (red dot at H) in the nematic, constitutes the topological dipole along HO. This dipole is associated with a flexo dipole along OH (violet arrow) or the midplane director $\mathbf{n}_M$ in the surrounding twisted nematic with $\mathbf{n}_B$ and $\mathbf{n}_T$ as the directors at bottom and top plates, respectively. In an external field $\mathbf{E}$, the flexodipole experiences a torque and the -1 hedgehog drifts so as to develop a component along $\mathbf{E}$ to lower the energy. If the sample were untwisted planar along $\mathbf{n}_M$, the drift would be along the great circle through H to a position such as A in a positive field and B in a negative field, the extent of drift increasing with $|U|$. But in the presence of the twist, to preserve the horizontal component of the flexodipole along the local director, the hedgehog has to move along the red and blue arrows depending on the field direction. Viewed from above, the defect appears to glide around the drop, clockwise or anticlockwise, depending on field direction.

fuse counterion layers next to the electrodes. Consequently, under steady conditions, the electric field in bulk, while remaining homogeneous, will be significantly diminished, and it rises rapidly towards the electrodes within the Debye-like screening layers [31]. In addition, when ions of one sign get preferentially adsorbed at the electrodes to form immobile surface charge layers with associated mobile counterion clouds, an intrinsic surface field E_i is established; E_i, which decays exponentially with distance z toward the midplane, when superimposed on an external electric field E_e, would render the overall surface field E_s enduringly asymmetric. The differing mobilities of the opposite charge carriers, by contrast, would lead to a surface field asymmetry that is transient [32]. Charge injection through imperfections in blocking layers would also contribute to this asymmetry [33]. When E_e is suddenly reversed to $-E_e$, as happens with SQW excitation, the equilibrium field distribution is altered in two time-dependent ways. The bulk field surges suddenly and transiently [34]. Secondly, the bulk field turns momentarily inhomogeneous and, in time, with the drift of counterion clouds, the inhomogeneity shifts toward the electrodes. These effects, augmented when intrinsic double layers are formed [35], produce favorable conditions for the development of various transient instabilities.

The instabilities in Fig. 6 may now be viewed in the light of aforementioned ionic effects. The periodic horizontal (H) domains appearing along $\mathbf{n}_T$, the rubbing axis at the top plate, whenever the applied field E_e switches to $-E_e$, would imply that positive ions are selectively adsorbed by the two electrodes; the resulting intrinsic field E_i, which is positive (negative) at the bottom (top) electrode, enhances the applied field $-E_e$ at the top electrode and lowers it at the bottom. Thus, the patterned state may be expected to evolve near the top substrate, provided the enhanced negative field therein is above the instability threshold. The modulation decays as the ions redistribute towards equilibrium. Further, the formation of domains parallel to $\mathbf{n}_T$ reveals their essential identity as the Bobylev-Pikin domains of flexoelectric origin [36–38]. This conclusion derives further support from (a) the increasing pattern period with decaying surface field (compare frames F_2 and F_3 of Fig. 6) and (b) observation of H stripes at successive voltage reversals in planar *untwisted* samples excited by SQW fields. The vertical (V) stripes formed at the switch from $-E_e$ to $+E_e$ is similarly explained. Then the momentary surge in the surface field occurs at the bottom electrode; it induces flexodomains oriented along y, appropriate to $\mathbf{n}_B$. It is important to note here the possible influence of dielectric torque on the overall distortion. The Freedericksz threshold determined at a high enough frequency (10 kHz) for ionic effects to be absent is 1.6 V for C-HB3 in the N-N_{TB} coexistence region, just below the onset temperature of the N_{TB} phase. However, due to ionic influence and lowered bulk field, this threshold is elevated considerably so that, even at a DC voltage below ± 4 V, no birefringence color change is seen in the nematic. However, when using an SQW field with $|U| = 2$ V, soon after a polarity reversal, the potential drop at the anode may be expected to considerably exceed this voltage so as to produce a homogeneous Freedericksz distortion. This would then superimpose on the periodic flexoinstability resulting in a hybrid flexodielectric reconfiguration of the director field.

Flexoelectrically induced dipole reorientation is readily observed in a 90° twist cell since the drift of the hyperbolic hedgehog around the N_{TB} drop appears, in planform, as a back and forth excursion along an arc in the xy plane. In planar untwisted nematic geometry, the displacement of the hedgehog is not as evident since it takes place in the xz plane with attendant defocusing effects being relatively less conspicuous. However, the interference pattern on the side of the hedgehog, as illustrated in Fig. 7 (video V3, SM [25]), does differ radically for positive and negative fields, indicating a corresponding shift in the focal plane of the hedgehog. More specifically, under sine-wave driving, while the birefringence colors within N_{TB} drops and in far-field nematic regions remain unaffected at all voltages, an extinction cross appears at the site of -1 defect at peak positive voltages (this cross, rotated relative to the axes of polarizers, is better seen in video V3), along with symmetrical interference fringes on either side of it. By contrast, at peak negative voltages, this cross is not seen; instead, bowlike interference bands appear across defect sites. As it appears from Figs. 7(a) and 7(c), positive (negative) fields shift the hyperbolic hedgehogs upward ($z > 0$) [downward ($z < 0$)]; this is an expected result when we consider the flexodipoles as directed opposite to elastic dipoles. These polarity-determined differences also point to
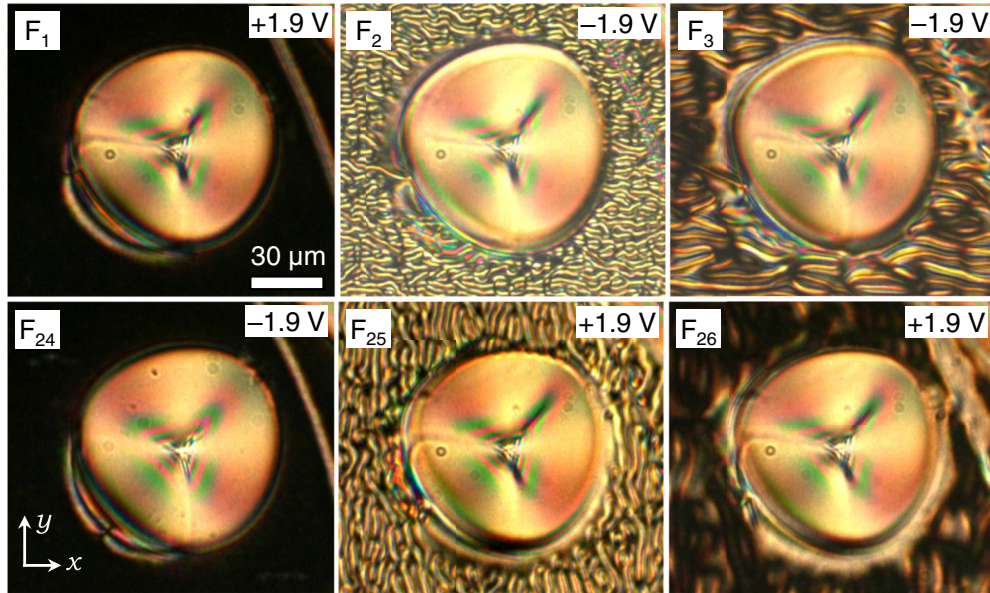
FIG. 6. Select frames F_i of a time series recorded with a 90° twisted layer of C-HB3 subjected to a SQW field ($f = 20$ mHz, $U = 1.9$ V) and viewed between parallel polarizers along y. The interval between frames is 1.08 s. In F_1, the field is positive, the -1 defect is shifted toward the horizontal, and the dark nematic matrix is structureless. In F_2, captured right after the field reversal, a pattern of horizontal stripes is seen in the nematic around the N_{TB} drop. The period of the pattern increases in time, as in F_3, and the nematic returns to the base state in a few seconds to remain undisturbed till the next polarity switch occurring soon after F_{24}; F_{25} again reveals a patterned nematic state, but now of vertical stripes, which decays by F_{27}. This sequence of instability is repetitive. $D_y = 83$ μm (F_1).

the deformations as *primarily* of flexoelectric, rather than dielectric, origin. A notable aspect of the deformations is their involved nature in that they are governed by both inverse and direct flexoelectric polarizations.

B. Flexodielectrically generated unidirectional transport of dipoles

In all our mixture samples, the normal Freedericksz threshold U_F measured at 10 kHz near the setting point of the N_{TB} phase is below 2 V; in the mHz frequency regime, due to electric double-layer effects and lowered bulk field, dielectric reorientation does not occur in the far-field ($\mathbf{n} \parallel \mathbf{x}$) N regions even at double this voltage. However, at hyperbolic defects of

elastic dipoles, reorientation in low-frequency fields becomes discernible even at ∼2 V (see Fig. 1, SM [25]). Since the curvature strains already present at defect sites favor Freedericksz destabilization, this reorientation may partly be of dielectric origin; in fact, we find that even in a high-frequency (1 kHz) field, at 1.5 V at which the far-field nematic remains planar, the -1 defect region shows slight changes in birefringence pattern. However, as evident from *polarity-sensitive* periodic changes in the director configuration of hyperbolic defects (Figs. 6 and 7), the deformation also involves flexoelectric polarization. The repetitively transient hydrodynamic backflows that accompany the growth and decay of the coupled flexodielectric distortions produce a propulsive force that leads
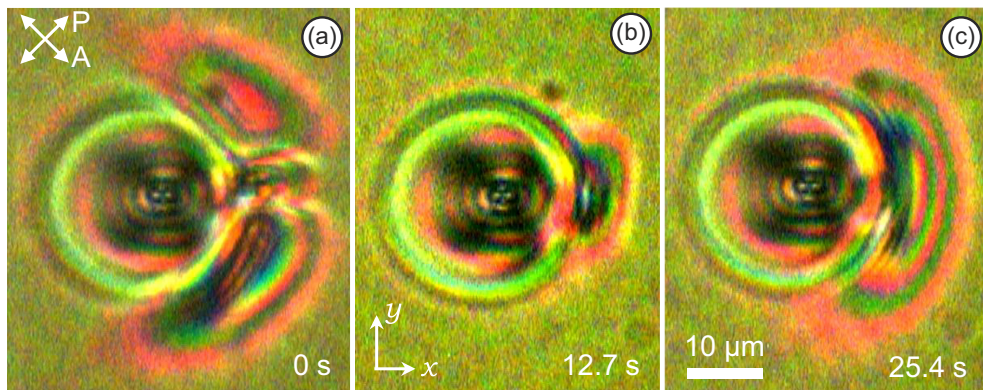

FIG. 7. Select frames of a time series recorded with a planar untwisted layer of C-OP3 in the N-N_{TB} biphasic region, subjected to a sine-wave field ($f = 0.02$ Hz, $U = 3.07$ V), showing the polarity-dependent effect on the -1 hedgehog. Interference pattern (a) at peak positive voltage, (b) just after the polarity change from positive to negative, and (c) at the peak negative voltage. Relative recording times are given in the lower right corner. $D_y = 29$ μm (a).
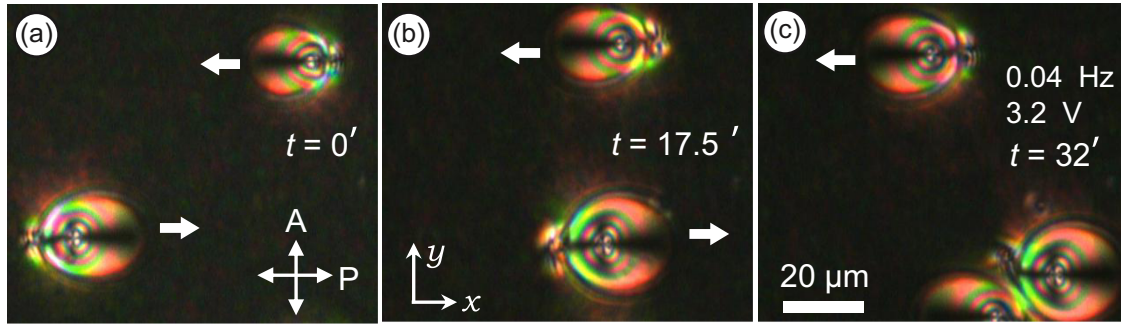
FIG. 8. Select frames of a time series showing oppositely drifting dipoles in a 20-μm-thick planar layer of C-OP3 subjected to a sine-wave field of frequency 0.04 Hz and rms voltage 3.2 V. Dark background is of nematic medium aligned along x. In (c), the lower of the two dipoles is coupled antiparallely to the one attracted to it from below. $D_y = 25.7\,\mu$m [(a), lower drop)].

to a transport of dipoles, which takes place on the average in the direction of their moments, the topologically positive drop always remaining in the lead (Fig. 8); video clips V4 and V5 (available in SM [25]) illustrate vividly the motion of parallel and antiparallel dipoles. Interestingly, when examined at small time intervals, the displacement shows sudden jumps (Fig. 9), each of which occurs soon after the voltage crosses its negative peak value and the corresponding maximum distortion begins to wane. At positive peak voltages the incremental displacement is rather mild. This asymmetry may have to do with the nature of coupling between flexo- and dielectric torques.

At any given frequency f of the applied field, the motion of dipoles is found to be uniform on the average, implying it as governed by a distance-independent force. In Fig. 10 illustrating this aspect, it is also seen that, for a drop of given size, the slope of the line $S_d(t)$, or the drift velocity v_d, increases with f; as shown in Fig. 11, this increase is again linear in f.
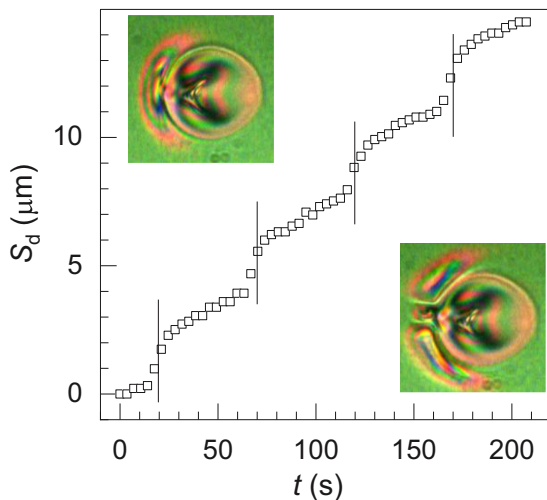
The drift speed of a dipole at fixed values of frequency and voltage is also dependent on the size of the N_{TB} drop, varying nearly linearly with the diameter as depicted in Fig. 12. By implication, the size of the distorted region around the -1 defect, which in turn depends on the size of the N_{TB} drop, influences the drift speed, with drops much smaller than L hardly showing any definitive motion.

It is important to clarify here the effect of the size of N_{TB} drops on the kinetics of dipoles, considering a wider range of D_y than represented in Fig. 12. Drops with $R > L$, which may reasonably be taken as flattened spheres, are associated with dipoles of lowered symmetry, C_{2v} in place of $C_{\infty v}$, similar to the dipoles created by certain shaped colloidal particles [39]. The dipoles formed of large drops are metastable and turn into quadrupoles eventually; significantly, the trace of Saturn rings surrounding them in their equatorial plane is seen all along the vertical diameter, indicating that thin nematic layers separate large drops from the bounding plates, obviating their
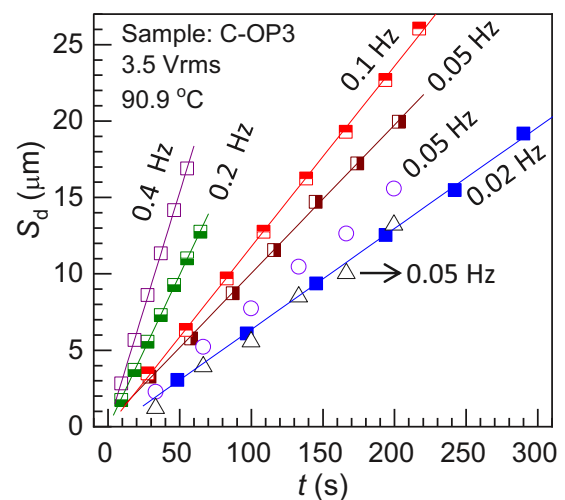

FIG. 9. Backflow-induced motion of a dipole in a planar nematic layer of C-OP3 at 91.9 °C. Displacement jumps occur at times indicated by vertical markers, just when the voltage begins to drop from its negative peak value; top inset shows the corresponding texture under diagonally crossed polarizers. Bottom inset shows the texture at the positive maximum voltage (midway between the time markers), at which the displacement increase is less conspicuous.

FIG. 10. Linear time dependence of displacement S_d of dipoles due to periodically varying flexodielectric distortion at hyperbolic hedgehogs. All squares (open, semifilled, or filled) represent the data from the same dipole with the N_{TB} drop measuring 30 μm along x; triangles and circles are for dipoles with their N_{TB} drops measuring, respectively, 20 and 25 μm along x. The rate of drift at a given frequency (0.05 Hz here) increases with increasing drop size.
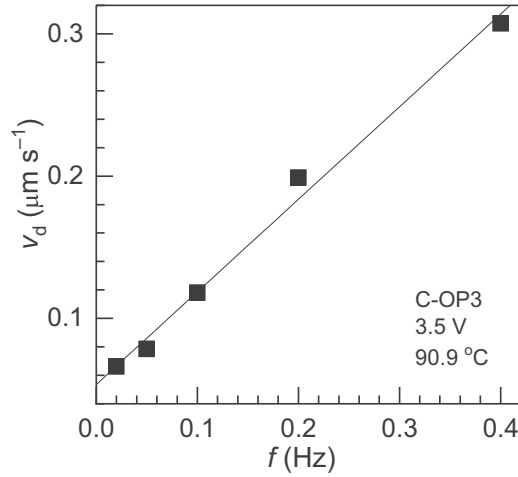
FIG. 11. Drift velocity v_d of a dipole as a linear function of frequency f of the applied field in a 20-μm-thick layer of C-OP3; planar cell at 90.9 °C.

FIG. 13. Drift velocity of dipoles as a function of applied voltage at different frequencies in a 20-μm-thick layer of C-TA5; planar cell at 91.3 °C. The continuous line for 0.5 Hz is a linear fit; the lines for 0.05 and 0.2 Hz are approximate fits to the equation $v_d = aU + bU^3$.

direct adhesion to the substrates; this conclusion also follows from the facile rotation of pairs of antiparallel dipoles, as described in our earlier paper (see Fig. 6 and video V2 of Ref. [24]). Dipoles with large drops ($D_y \geqslant 2$ L) also exhibit the drift motion, but with reduced velocity compared to that corresponding to the linear trend in Fig. 12; for example, a drop with $D_y = 40\,\mu$m, with other parameters just as in Fig. 12, is found to drift with $v = 0.085\,\mu$m/s (see Fig. 2 in SM [25]); similarly, the drop in video V3 which measures 48 μm along y is seen to drift along -x; the measured velocity of this motion is 0.034 μm/s. The quadrupoles, understandably, do not show the drift. Dipoles with large N_{TB} drops, instead of transforming into quadrupoles, may remain dipoles and also grow ever increasingly through a systematic evolution of disclinations, as discussed in Ref. [24]. In such large dipoles,
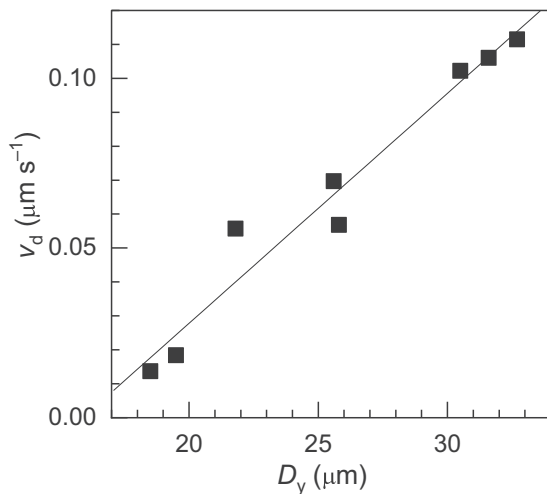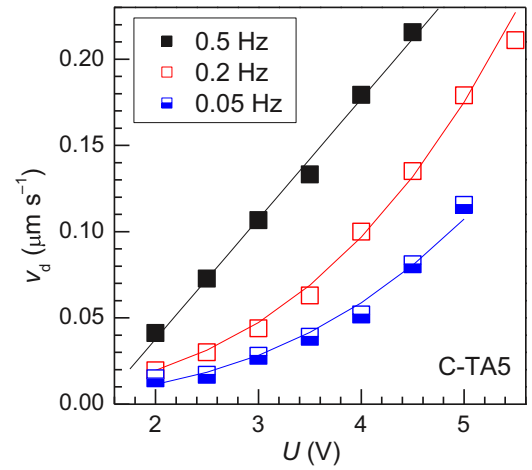

FIG. 12. Drift velocity of dipoles as a function of the principal axis D_y along y of the N_{TB} drops in a 20-μm-thick layer of C-OP3 subjected to a sine-wave field with $f = 0.04$ Hz and $U = 4$ V. Planar nematic cell at 90.5 °C.

electric field generates multiple disclinations accompanied by complex shape changes that need a separate detailed study.

Predictably, the drift of dipoles is accelerated under an increasing voltage. At 0.5 Hz, v_d is linear in U; at lower frequencies, as the results for 0.05 and 0.2 Hz in Fig. 13 would indicate, the $v_d(U)$ plot is slightly nonlinear, with the data largely agreeing with the relation $v_d = aU + bU^3$. If the motion of the dipole were to be governed exclusively by dielectric backflows, one would have expected v_d to vary as U^2, since the dielectric torque is a quadratic in the field. This is one of the reasons for considering the drift as due to flexodielectric backflows. Our data in Fig. 13 are limited by the positive dielectric anisotropy of the mixtures, which restricts the voltage to be below the Bobylev-Pikin threshold of the surrounding nematic. We plan to prepare a dielectrically negative mixture to study the dipole drift over a wider voltage range and to better ascertain the nature of variation of $v_d(U)$.

In 90° twisted layers, the dipole drift shows the same features as in planar untwisted layers except that the motion takes place, on the average, along the diagonal line along which $\mathbf{n}_M$ lies, as in Fig. 14 (video V6, SM [25]). In our study of the motion of several dipoles in twist cells, we have always found the x and y components of displacement, S_x and S_y, to be linear in time, although the slopes of straight lines $S_x(t)$ and $S_y(t)$ often varied. Thus, the dipoles, while remaining uniform in their drift, often deviate from following a strictly diagonal course (Fig. 15). This is mainly due to interaction with other dipoles in the vicinity.

Flexoelectric influence on the geometry of an isolated dipole assumes a more complex form for a bound pair of antiparallel dipoles in a twisted nematic matrix. As a comparison of Figs. 16(a) and 16(b) would show, the pair rotates clockwise in a positive field; the line joining the N_{TB} drops tends toward x as U increases, the effect becoming particularly noticeable above ~ 3 V. The rotation is rather slow, taking several minutes to reach the steady state. The sense of rotation reverses for negative voltages [Fig. 16(c)]. Additionally, above the threshold of the Bobylev-Pikin (BP) volume instability,
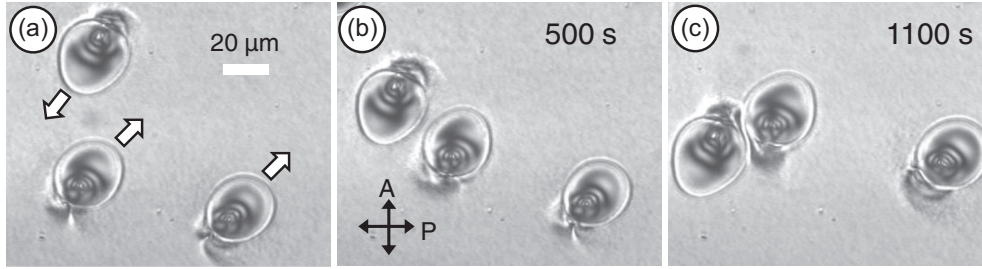
FIG. 14. Select frames of a time series recorded using laser scanning microscopy, showing the drift of a dipole nearly along a diagonal in a 90° twisted layer of C-HB3 subjected to a sine-wave field with $f = 0.04$ Hz and $U = 2.6$ V. The time stamps in (b) and (c) are relative to (a). $D_y = 24\,\mu$m [(a), right side drop].

a striking feature appears in the form of the breaking and drifting apart of the bound pair of N_{TB} drops; in Fig. 16(d) (see video V7 in SM [25]) this drift occurring along the periodic BP domains under a negative voltage is illustrated. Upon slowly reducing the field to zero (rapid changes in U involve complicated surface distortions due to ion transport that decouple the N_{TB} dipoles), the separated dipoles move backward, approaching each other and, eventually, returning to the base configuration, as in Fig. 16(e) (see video V8 in SM [25]). Above -4 V, the periodic BP domains evolve diagonally in the surrounding twisted nematic, as in Fig. 16(f) for -5 V. It is to be noted that even after removing the field, the domain connecting the N_{TB} drops remains intact. The separation of the two drops is a linear function of time in both field-on and field-off states (Fig. 17). These results indicate that the BP instability originates in the region of contact between the paired N_{TB} drops at a voltage slightly lower than that for the far-field nematic, as evident in Fig. 16(c). The drifting apart of the dipoles allows for the growth of energetically favorable BP domain that links the two drops and becomes a part of the periodic pattern at higher voltages.

It is interesting to compare the dipole transport generated flexodielectrically (this study) with that brought about by other mechanisms. For example, in the dielectrically driven case [19,20], the mass transport in the entire fluid nematic matrix due to a large applied voltage (U about 10 times the dielectric threshold) powers the translation of small particles ($R \ll L$) with a velocity on the order of $1\,\mu$m s^{-1}. At such high voltages, the director field around the hyperbolic defect would be strongly deformed in favor of homeotropic alignment. In our study, the large N_{TB} drops (often of size more than L in the layer plane), along with their counter defects, travel with velocities an order lower, driven by transient deformations and backflows confined only to the $\mathbf{n}$ field of hyperbolic defects. In Ref. [19], opposite polarities of splay Freedericksz deformation near the two substrates lead to a bidirectional (along $\pm\mathbf{n}$) drift of particles levitated to the wall regions, with the -1 defect leading the way in either case. By contrast, as a rule, the net drift of dipoles due to N_{TB} drops of large size takes place in the opposite direction (-1 defect trailing) for all dipoles (along $\pm x$ in planar cells and $\pm\mathbf{n}_M$ in TN cells), with small N_{TB} drops ($D_y \approx 10\,\mu$m) hardly moving (see Fig. 12). Evidently, the nature of backflow-related motion also depends on the transient response times and the combined flow rate from both the on and off states. For the dielectric case [19], the rise and decay time constants are on the order of 1 ms and 1 s, respectively. In the flexoelectric case, some previous results indicate both the response times to be on the order of 50 ms [40]. The low frequency of the fields used in this study allows for the reorientation and relaxation processes to be complete in both flexoelectric and dielectric cases.

Another important particle transport mechanism is electrophoresis that relies on electric charges gathered at defects or double layers formed at interfaces. In the so-called liquid-crystal enabled nonlinear electrophoresis driven by AC fields, the flow velocity can assume any direction relative to the electric field. In experiments involving dielectrically negative nematics and an in-plane field $\mathbf{E} \perp \mathbf{n}_o$, flow velocities with components both along and normal to $\mathbf{n}_o$ have been observed [22,23]. In our experiments, since the dipole displacement is directly observed to accompany the distortion growth and decay (Fig. 9), electrophoresis does not appear to play a significant role.

Before concluding, it is relevant to make a mention of an earlier numerical simulation study of backflow in a nematic liquid crystal that acts as a weak electrolyte and undergoes inverse flexoelectric distortion upon application or removal of a step voltage [21]. The analysis considers the system as one dimensional and uses the equations for balance of torques on the director and ion transport, along with the Poisson and Navier-Stokes equations. It concludes that, in a deformed
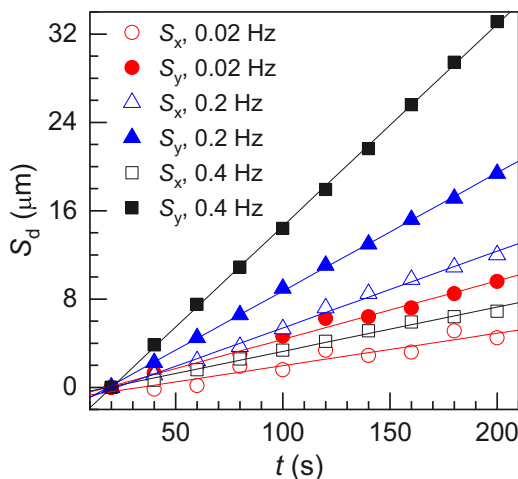

FIG. 15. Linear time variation of x and y components of displacement of dipoles at different frequencies of the applied sine-wave field with the voltage $U = 2.8$ V.
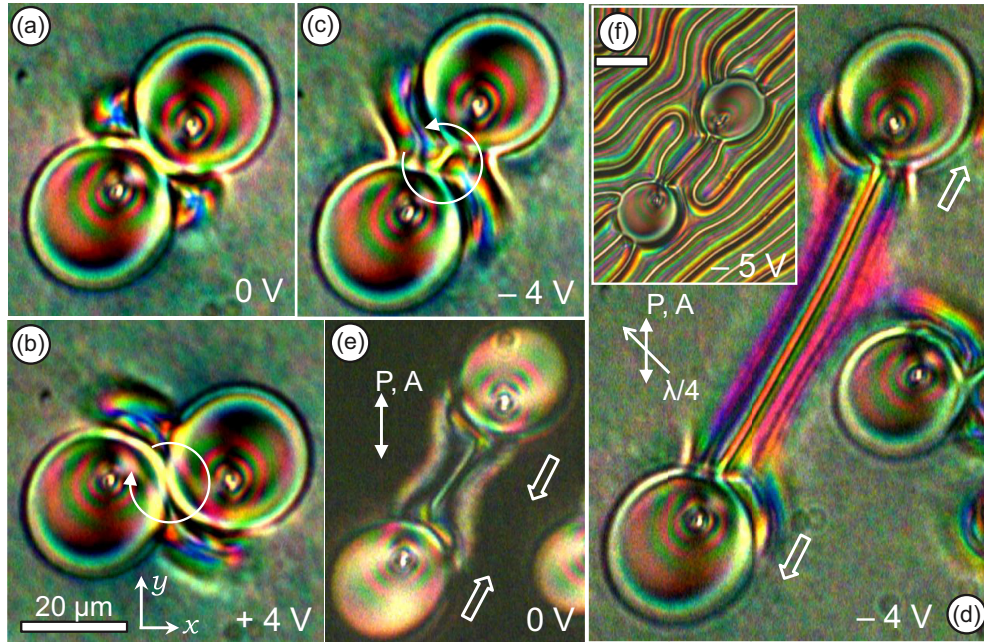
FIG. 16. Effect of static fields on bound antiparallel dipoles in a 90° twisted nematic layer of C-HB3. Curved arrows in (b), (c) indicate rotational sense; block arrows in (d), (e) show the direction of drift of the drops. Scale bar is common in (a)–(e). Parallel polarizers, $P(90)$–$A(90)$, are used with a quarter-wave plate in all frames but (e). $D_y = 28\,\mu$m [(a), upper drop of the dimer].

planar layer, flexoelectricity leads to a strong asymmetry of director distribution about the midplane; the peak backflow velocities v_p that occur in the midplane $z = 0$ (and are on the order of 1–$100\,\mu$m s^{-1}) differ greatly for the rise and decay modes, with v_{pd} for the decay being several times v_{pr} for the rise. Going by these results, it is reasonable to expect a unidirectional dipole drift in a layer in which repetitive growth and

decay of distortion occur under a slowly varying sine-wave field of suitable voltage amplitude.

IV. CONCLUSIONS

A binary mixture made mainly of the twist-bend nematogen CB7CB and a small quantity of a surfactant material behaves as a nematic colloid in the N-N_{TB} biphasic region. The N_{TB} phase separates from the nematic matrix in the form of droplets that act as radial hedgehogs and generate hyperbolic counter defects in their vicinity, in the nematic fluid. The resulting topological dipoles have been found to interact with an external electric field mainly through dielectric and flexoelectric couplings. More specifically, in planform, the hyperbolic defect in a TN cell, when excited by a low frequency sine-wave field, appears to execute coherent oscillatory motion about its mean position, along an arc in the xy plane; in reality, it always tends toward the negative electrode, while keeping itself in the plane of the local director and the field. In a planar cell, the defect moves back and forth about its mean position and along an arc in the xz plane. These results are attributable to direct flexoelectric polarization developed in a direction opposite to the elastic dipole. In addition, the dipole as a whole exhibits a uniform translatory motion parallel to itself, with the N_{TB} drop leading the way. From the displacement increments at small time intervals taking place in jumps, dependence of drift velocity v_d on size of the N_{TB} drops, and nonquadratic variation of v_d with voltage, we conclude the dipole drift as due to backflows associated with periodic growth and decay of coupled flexodielectric distortions. The role of flexoelectricity can possibly be better understood using a dielectrically negative mixture suitable for dipole formation, and efforts are on to prepare such a mixture.
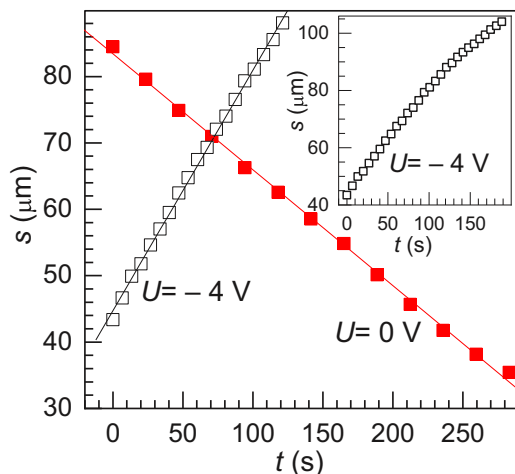

FIG. 17. Time variation of the separation s between two coupled N_{TB} drops. The E-on data (open squares) are for t from 0 to 120 s, in which interval the drift remained relatively free of interference from surrounding drops; in the inset showing the data for a wider time range, the drift is seen decelerated in later stages due to other drops in the path of the drifting one at the top. For an isolated bound pair of drops, $s(t)$ is linear both in E-on and E-off states, with the motion in the on state twice as fast as that in the off state.

ACKNOWLEDGMENTS

[1] R. B. Meyer, Mol. Cryst. Liq. Cryst. **16**, 355 (1972).

[2] I. Muševič, *Liquid Crystal Colloids* (Springer, Cham, Switzerland, 2017).

[3] H. Stark, Phys. Rep. **351**, 387 (2001).

[4] M. Kleman, *Points, Lines and Walls in Liquid Crystals, Magnetic Systems and Various Ordered Media* (Wiley, Chichester, England, 1983).

[5] R. Pratibha and N. V. Madhusudana, Mol. Cryst. Liq. Cryst. **178**, 167 (1990).

[6] E. Terentjev, Phys. Rev. E **51**, 1330 (1995).

[7] P. Poulin, H. Stark, T. C. Lubensky, and D. A. Weitz, Science **275**, 1770 (1997).

[8] I. Muševič, M. Škarabot, U. Tkalec, M. Ravnik, and S. Žumer, Science **313**, 954 (2006).

[9] U. Tkalec, M. Ravnik, S. Čopar, S. Žumer, and I. Muševič, Science **333**, 62 (2011).

[10] T. Araki and H. Tanaka, Phys. Rev. Lett. **97**, 127801 (2006).

[11] S. Copar, U. Tkalec, I. Muševič, and S. Žumer, Proc. Natl. Acad. Sci. USA **112**, 1675 (2015).

[12] A. Nych, U. Ognysta, M. Škarabot, M. Ravnik, S. Žumer, and I. Muševič, Nat. Commun. **4**, 1489 (2013).

[13] P. Poulin, V. Cabuil, and D. A. Weitz, Phys. Rev. Lett. **79**, 4862 (1997).

[14] T. Lubensky, D. Pettey, N. Currier, and H. Stark, Phys. Rev. E **57**, 610 (1998).

[15] O. P. Pishnyak, S. V. Shiyanovskii, and O. D. Lavrentovich, J. Mol. Liq. **164**, 132 (2011).

[16] I. Lazo and O. D. Lavrentovich, Philos. Trans. Royal. Soc. A **371**, 20120255 (2013).

[17] G. Liao, I. I. Smalyukh, J. R. Kelly, O. D. Lavrentovich, and A. Jákli, Phys. Rev. E **72**, 031704 (2005).

[18] S. A. Tatarkova, D. R. Burnham, A. K. Kirby, and G. D. Love, Phys. Rev. Lett. **98**, 157801 (2007).

[19] O. P. Pishnyak, S. Tang, J. R. Kelly, S. V. Shiyanovskii, and O. D. Lavrentovich, Phys. Rev. Lett. **99**, 127802 (2007).

[20] O. P. Pishnyak, S. V. Shiyanovskii, and O. D. Lavrentovich, Phys. Rev. Lett. **106**, 047801 (2011).

[21] M. Buczkowska and G. Derfel, Liq. Cryst. **41**, 169 (2014).

[22] O. D. Lavrentovich, Soft Matter **10**, 1264 (2014).

[23] O. D. Lavrentovich, Curr. Opin. Colloid Interface Sci. **21**, 97 (2016).

[24] K. S. Krishnamurthy, D. S. Shankar Rao, M. B. Kanakala, C. V. Yelamaggad, and M. Kleman, Soft Matter **16**, 7479 (2020).

[25] See Supplemental Material at http://link.aps.org/supplemental/10.1103/PhysRevE.103.042701 for video clips V1.avi–V8.avi, some optical textures, and related notes in SM.pdf.

[26] R. B. Meyer, Phys. Rev. Lett. **22**, 918 (1969).

[27] K. S. Krishnamurthy, Phys. Rev. E **92**, 032504 (2015).

[28] K. S. Krishnamurthy, Phys. Rev. E **89**, 052508 (2014).

[29] K. S. Krishnamurthy, P. Kumar, and M. V. Kumar, Phys. Rev. E **87**, 022504 (2013).

[30] K. S. Krishnamurthy, Phys. Rev. E **88**, 062503 (2013).

[31] G. Barbero, D. Olivero, N. Scaramuzza, G. Strangi, and C. Versace, Phys. Rev. E **69**, 021713 (2004).

[32] R. N. Thurston, J. Cheng, R. B. Meyer, and G. D. Boyd, J. Appl. Phys. **56**, 263 (1984).

[33] S. Lu and D. Jones, Appl. Phys. Lett. **16**, 484 (1970).

[34] M. Scalerandi, P. Pagliusi, G. Cipparrone, and G. Barbero, Phys. Rev. E **69**, 051708 (2004).

[35] K. S. Krishnamurthy and P. Kumar, Liq. Cryst. **34**, 257 (2007).

[36] Y. P. Bobylev and S. A. Pikin, Sov. Phys. JETP **45**, 195 (1977); Y. P. Bobylev, V. G. Chigrinov, and S. A. Pikin, J. Phys. (Paris) **40**, C3-331 (1979).

[37] S. A. Pikin, *Structural Transformations in Liquid Crystals* (Gordon and Breach, New York, 1991).

[38] L. M. Blinov and V. G. Chigrinov, *Electrooptic Effects in Liquid Crystal Materials* (Springer, Berlin, 1994), Chap. 4.

[39] S. Park, Q. Liu, and I. I. Smalyukh, Phys. Rev. Lett. **117**, 277801 (2016).

[40] G. Derfel and M. Buczkowska, Liq. Cryst. **40**, 272 (2013).